Physica Medica 66 (2019) 45–54

Contents lists available at ScienceDirect

Physica Medica

journal homepage: www.elsevier.com/locate/ejmp

Original paper

Experimental benchmarking of Monte Carlo simulations for radiotherapy dosimetry using monochromatic X-ray beams in the presence of metal-based compounds

Jenny Spiga[a,*], Paolo Pellicioli[b,c,d], Sam P. Manger[e], Jon A. Duffy[a], Alberto Bravin[b]

[a] Department of Physics, University of Warwick, UK
[b] European Synchrotron Radiation Facility, Grenoble, France
[c] Grenoble Alpes University, France
[d] Swansea University, UK
[e] School of Chemical Engineering, University of Birmingham, UK

ARTICLE INFO

Keywords:
Monte Carlo simulations
Radiotherapy
Dosimetry
Dose enhancement
X-rays

ABSTRACT

The local dose deposition obtained in X-ray radiotherapy can be increased by the presence of metal-based compounds in the irradiated tissues. This finding is strongly enhanced if the radiation energy is chosen in the kiloelectronvolt energy range, due to the proximity to the absorption edge. In this study, we present a MC application developed with the toolkit GEANT4 to investigate the dosimetric distribution of a uniform monochromatic X-ray beam, and benchmark it against experimental measurements. Two validation studies were performed, using a commercial PTW RW3 water-equivalent slab phantom for radiotherapy, and a custom-made PMMA phantom conceived to assess the influence of high atomic number compounds on the dose profile, such as iodine and gadolinium at different concentrations. An agreement within 9% among simulations and experimental data was found for the monochromatic energies considered, which were in the range of 30–140 keV; the agreement was better than 5% for depths < 60 mm. A dose enhancement was observed in the calculations, corresponding to the regions containing the contrast agents. Dose enhancement factors (DEFs) were calculated, and the highest values were found for energies higher than the corresponding K-edges of iodine and gadolinium. The *in-silico* results are in line with the empirical findings, which suggest that GEANT4 can be satisfactorily used as a tool for the calculation of the percentage depth dose (PDD) at the energies considered in this study in the presence of contrast agents.

1. Introduction

Radiation therapy (RT) is one of the most common and efficient treatments of cancer, and it makes use of ionising radiation to cause lethal damage to the tumoral cells by damaging the cellular DNA. The efficacy of RT can be increased if the tumour is previously loaded with high atomic number (Z) compounds and then irradiated with X-rays in the kiloelectronvolt energy range. In this case, the local dose deposition is enhanced because the effective Z of the tumour is increased compared to the adjacent tissues. X-rays are preferentially stopped by high-Z elements due to the larger photoelectric cross section ($\propto Z^4$) compared to tissue/water, with the emission of electrons, which contribute to the local dose deposition in the vicinity of the high-Z atoms. K-shell vacancies created during the absorption process are filled with higher orbital electrons, leading to the generation of either Auger electrons, which have a short mean free path and are deposited locally, or fluorescent X-rays, which escape from the original target zone. Both phenomena produce a dose enhancement in the tumour volume without damaging the surrounding tissues [1,2], with a consequent increase of the probability of tumour control [3–5]. Two natural candidates as dose enhancers are gadolinium and iodine, which are both high-Z, biologically-compatible elements, already used in magnetic resonance imaging (MRI) and in diagnostic X-ray imaging. Historically, the use of gadolinium-based (Z = 64) contrast agents for MRI dates back to the 1980s, when gadopentetate dimeglumine (Magnevist®) became available for clinical use. Since then, eight further gadolinium chelates have been developed and approved in many regions worldwide, including the gadobutrol (Gadovist®), which has twice the concentration of other contrast agents (1.0 M). Iodine-based (Z = 53) contrast agents were first used in the 1920s with the development of

* Corresponding author.
E-mail address: j.spiga@warwick.ac.uk (J. Spiga).

https://doi.org/10.1016/j.ejmp.2019.09.075
Received 4 February 2019; Received in revised form 3 August 2019; Accepted 11 September 2019
Available online 23 September 2019

sodium iodide. Today, a number of such contrast agents (both ionic and non-ionic, and mono- and two-ring structures) are approved for medical use and are administered clinically world-wide, i.e.: iohexol (Omnipaque™, GE Healthcare), iopromide (Ultravist™, Bayer Healthcare), iodixanol (Visipaque™, GE Healthcare), ioxaglate (Hexabrix™, Mallinckrodt Imaging), iothalamate (Cysto-Conray II™, Mallinckrodt Imaging), and iopamidol (Isovue™, Bracco Imaging). Such contrast agents are used with the aim to enhance the image contrast between highly vascularized and neighbouring tissues.

A particular case is encountered when the high-Z material is associated to a chemotherapic drug. Such drugs become photoactivable when irradiated with monochromatic X-rays at energies just above the K-edge of the metal, which for most elements occurs at energies < 100 keV. For this to happen in practice, X-ray beams of the suitable energy and with a sufficiently high fluence, such as the ones available at synchrotron radiation facilities, have to be used. When tissues are irradiated with conventional radiotherapy units (mean photon energies > 1 MeV) the photoactivation would only marginally contribute to the local dose deposition, because the Compton scattering would replace the photoelectric effect as main X-ray interaction depositing dose. This effect was confirmed by a study from Zhang *et al.*, where an almost negligible dose enhancement by gadolinium was found when using megavoltage external beams involved in clinical radiotherapy [6]. 4 and 6 MeV Linac beams filtered with low-Z targets such as beryllium and aluminium were considered by Robar in order to produce an energy spectrum more suitable for contrast enhanced radiation therapy. They found an increase in the relative population of photons in the vicinity of the K-edge of iodine, although the magnitude of dose enhancement cannot be expected to reach that for kilovoltage X-ray beams [7].

Intense, highly monochromatic X-ray beams at energies up to 100 keV are available at the ID17 biomedical beamline of the European Synchrotron Radiation Facility (ESRF) in Grenoble, where different photoactivation protocols have been studied; additionally, some molecular and cellular mechanisms involved in metal-based chemotherapy plus synchrotron radiation (SR) have been identified [8–13]. In all protocols, the critical point is the possibility of loading biocompatible high-Z drugs at a sufficiently high concentrations to determine a significant increase of the local dose deposition into the tissues.

Monte Carlo (MC) simulations are the method of preference to predict the dose distribution determined by the presence of metals. Back in 1992, Solberg *et al.* [14] developed a Monte Carlo application based on the MCNP4 code to calculate the radiation dose enhancement factors (DEF) in the therapy of brain tumours using iodinated contrast agents. They studied the factors that influence the DEFs and suggested that higher DEFs can be achieved using monochromatic beams with energies near the K-edge of iodine or gadolinium. Verhaegen *et al.* [15] investigated with the BEAMnrc MC code the influence of different kiloelectronvolt spectra when used with a range of clinically achievable gadolinium and iodine concentrations. The experimental validation of their calculations was performed using a polychromatic X-ray beam at 120 kVp irradiating contrast media solutions placed between two PMMA slabs and measuring the dose at different depths using unlaminated radiochromic films [16]. In terms of beam size, a Monte Carlo study conducted with the PENELOPE and the GEANT4 codes, respectively reported gadolinium and tantalum as a very suitable dose enhancer in microbeam radiation therapy applied to brain tumours [17–19].

In this work, we analysed the suitability of Geant4 for depth dose studies using a homogeneous X-ray monochromatic beam in the kiloelectronvolt energy range. We also investigated on the Geant4 performances in dose enhancement simulations when using clinically accepted contrast agents (iodine and gadolinium) at different concentrations. Both cases are yet missed in the literature and are of primary importance in view of the on-going developments for dose-enhanced radiotherapies using monochromatic and polychromatic X-rays in the kiloelectronvolt energy range. We considered the depth dose reduction in the regions adjacent to the contrast agent regions, and compared the simulated results with experimental measurements collected at the biomedical beamline ID17 of the ESRF. The final goal is to have a benchmarked application to be used in future depth dose studies at low energies in the presence of contrast agents, which will be then extended to the use of polychromatic radiation and micrometer-sized beams.

2. Materials and methods

2.1. Geant4 simulation setup and choice of parameters

Geant4 is a Monte Carlo toolkit widely used in dose calculations thanks to the well-validated physics models, powerful geometry modelling tools, and convenient visualization utilities. We used version 10.4, which includes an updated database for electromagnetic low energy physics. In particular, we used the G4EmStandardPhysics_option4 electromagnetic physics libraries that contain a selection of the most accurate standard and low energy models available in Geant4; they are therefore recommended for medical applications [20]. The General Particle Source (GPS) class allowed the definition of the source energy, position and size. To calculate the PDD in the phantom we used monochromatic energies in the range 30–140 keV; the X-ray beam was simulated as a homogeneous planar source of 2×2 cm^2 impinging perpendicularly on the phantom. A total of 10^9 incident photons were simulated. The range cut was set to 1 μm, with a low energy limit for secondary particles production of 250 eV. Geant4 contains a command-based, built-in scoring mesh that allows the user to divide the phantom in a three-dimensional array of voxels, and score commonly used physics quantities such as the absorbed dose. We used a voxel size of $10 \times 10 \times 5$ mm^3 (XxYxZ, with Z along the beam propagation) in the first part of the study, and $10 \times 10 \times 1$ mm^3 in the dose enhancement analysis. The voxel size was chosen to sample a uniform beam along the XY plane and to fit the dimension of the sensitive volume of our ionization chamber along the incoming beam propagation axis (Z). The uniformity within XY was verified for each energy by using a Germanium line detector [21]; the measured beam homogeneity within the 10×10 mm^2 surface was better than 1%. The phantoms simulated have the same shape, dimensions and materials of those used in our experiments, which are represented in Fig. 1A and B and will be described in the following paragraphs. The metal-based compounds have been simulated at different concentrations, defining the compound density and the fractional mass of each component. Values have been chosen in agreement with the effective measured mass concentrations as described in Section 2.3.

2.2. The ID17 beamline and the beam harmonics content estimation

The experiments were performed at the ID17 biomedical beamline of the ESRF. The beamline originates from a wiggler source (10 full periods; period length: 150 mm). The generated X-ray beam is filtered by permanent absorbers (Be: 2.0 mm; C: 0.5 mm; Al: 0.5 mm) before reaching the double Si(1 1 1) bent Laue crystal monochromator [22] which allows to select a working energy in the interval 25–140 keV. The beam can be shaped using three different sets of remotely controlled tungsten slits, which attenuate and absorb the beam not passing through the aperture. The sample was positioned on a remotely controlled platform placed in the experimental hall (starting at about 145 m from the source), which allows positioning and scanning the sample through the beam with micrometric precision. The X-ray beam is transported in ultra-high vacuum until the last Kapton window, located ~ 8 m upstream from the sample. In the case of the Si(1 1 1) reflection, also third- and eventually fourth-order harmonics might contaminate the beam diffracted by the crystal monochromator; second-order harmonics are, in fact, not allowed by the selection rules for the

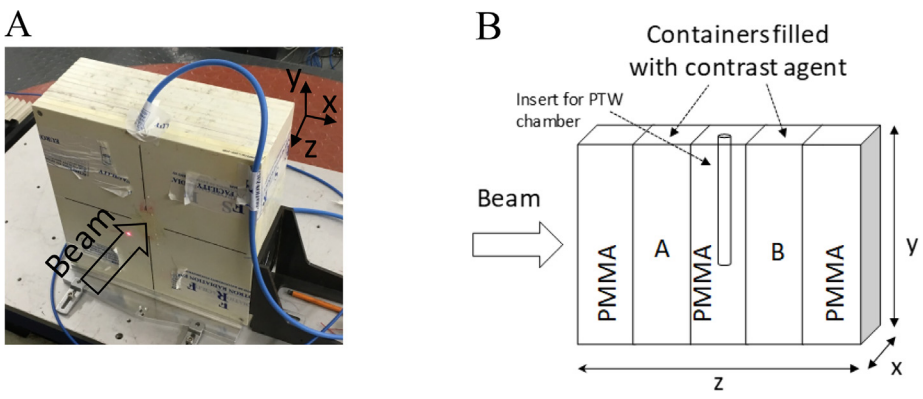

Fig. 1. Phantoms used experimentally. (A) photo of the PTW RW3 water-equivalent slab phantom at the ESRF with the PTW chamber inserted. (B) Schematic diagram of the phantom used to measure the difference in dose deposition with the contrast agent. The two containers A and B, placed in between the PMMA blocks, were filled with the metal-based compounds. One of the PMMA blocks had a cavity to allow the insertion of a PTW 31010 semiflex chamber. The blocks and containers were detached and could be positioned in different sequences in order to reproduce different geometries.

silicon crystal structure [22]. For the irradiations at 30 and 35 keV, a wiggler gap of 60 mm was used, corresponding to a maximum field of 0.61 T, while, for 40 keV, the gap was set to 56 mm, corresponding to a magnetic field of 0.68 T. By using the XOP software [23] the flux was calculated at the fundamental energy (30 keV, 35 keV, 40 keV) and the third- and fourth-order harmonics (respectively 90 keV and 120 keV; 105 keV and 140 keV; 120 keV and 160 keV) delivered by the source. The photon fluxes were then transported through the permanent absorbers and the 8 m of air by using the X-ray mass attenuation coefficients provided by the NIST databases [24]. Finally, the values were scaled by the reflectivity curve size of the crystal at the different energies. The reflectivity power for the third- and the fourth-order harmonics were estimated in 3 and 4, respectively [22]. The calculated values of third and fourth harmonic contaminations of the X-ray beam delivered by the monochromator were used as inputs for the Monte Carlo calculations reported in Section 2.3.

2.3. Benchmarking of the GEANT4 simulations with solid water phantom dosimetry

In our experiment, the depth dose profiles deposited by monochromatic X-ray energies ranging from 30 to 140 keV have been measured and compared with the calculated dose profiles. A PTW RW3 water-equivalent slab phantom with dimensions of 30 × 30 × 12 cm^3 (Fig. 1A) has been employed. The phantom contained a plate with a recess to hold an ionisation chamber. Solid water phantoms are often used as water substitute in dosimetry calibration, quality assurance, and patient-specific output measurement [25,26]. For real-time dosimetry measurements, a PTW 31010 semiflex ionisation chamber with a sensitive volume of 0.125 cm^3 was used. The slabs (typically 0.5–1 cm thick) could be recombined in order to move the ionisation chamber and evaluate the dose deposited at different depths. A second set of experimental data was collected using EBT3 Gafchromic™ films [27]. The dynamic range of this type of film is 0.2–20 Gy, making it suitable for many medical applications. Unlike an ionisation chamber, the Gafchromic film does not give a real-time dose measurement, as it contains colourless dyes that become blue after X-ray exposure due to radiation-induced polymerisation; this chemical conversion requires about 24 h for its full development. For an accurate film dosimetry, three sets of calibration films were irradiated at three different energies (30, 50 and 100 keV), delivering a dose of 0, 0.5, 1.0, 2.0, 5.0, 10.0 and 15.0 Gy for each energy. Based on these curves, calibration curves (not shown) were established to estimate the unknown doses in the irradiated films. After irradiation, the film was scanned with an EPSON V750 scanner and the optical density was determined with MATLAB. The entrance dose delivered experimentally was 2.0 Gy for measurements using the PTW chamber and 10.0 Gy with the EBT3 film.

2.4. Experimental dosimetry with dose enhancers

The contributions of iodine (10 mg/ml) and gadolinium (4 mg/ml) to the PDD within the sample were examined. The compositions have been measured by a certified laboratory for chemical analyses (FILAB, Dijon, France); the simulations have been performed based on the effective measured mass concentrations. Our custom-made phantom had a size of 50 × 50 × 88 mm^3 (Fig. 1B), and was made of three PMMA blocks interspersed with two containers (each 14 mm thick) filled with the dose enhancers. One of the three blocks of PMMA had a cavity allowing the insertion of a PTW 31010 semiflex chamber, so measurements could be acquired at different depths. The experimental energies were determined considering the K-edge binding energy of the two metals used, which are 33.17 keV for iodine and 50.24 keV for gadolinium. Monochromatic energies of 30 keV, 35 keV, 45 keV, 55 keV and 75 keV were employed. The nominal entrance dose delivered was 5 Gy. Before each set of measurements (i.e. for each monochromatic energy used), the block containing the ionization chamber on its own was irradiated to verify the accuracy of the entrance dose; for this purpose the protocol described in Prezado *et al.* [28] was used. Due to limitations in the dose measurement devices at our disposal (thickness of the ionisation chamber), multiple empirical data at different depths inside the high-Z solution were not acquired.

2.5. Determination of uncertainties

The uncertainty in the ionisation chamber measurements has been assumed to be ± 5% for energies up to 75 keV and ± 2% for higher energies; these are the maximum errors reported in the ionisation chamber specifications combined with the uncertainty of the chamber calibration. To reduce the chamber statistical error during the experiment, the mean value obtained after repeating each measurement three times was considered. The statistical uncertainty in the film measurements has been calculated following the methodology developed by Devic *et al.* [29]. The film was calibrated such that the optical density was fitted as a function of dose to the film, using the form

$$Dose = a \times netOD + b \times netOD^n \quad (1)$$

where a, b and n are determined using a least square fit. The sigma uncertainties on a, b and n were then considered by taking the square root of the diagonal values of the covariance matrix from the fit. The percentage uncertainty on the dose measurement was then calculated by using the following formula:

$$\sigma_D(\%) = \frac{\sqrt{netOD^2 \cdot \sigma_a^2 + netOD^{2n} \cdot \sigma_b^2 + (a + n \cdot b \cdot netOD^{n-1}) \cdot \sigma_n^2 \cdot netOD}}{D} \cdot 100 \quad (2)$$

Table 1
Harmonic content in percentage at the entrance of the phantom. In the experiment, for energies of the fundamental above 40 keV, the harmonic content is negligible (< 0.3%).

Energy of the fundamental (keV)	Third-order harmonic content (in %)	Fourth-order harmonic content (in %)
30	2.2	0.3
35	1.1	0.1
40	0.9	0.08

3. Results

3.1. Calculation of the harmonics

The calculated third- and fourth-order harmonic contents at the entrance of the phantom are reported in Table 1. The values were derived following the procedure described in Section 2.2. These values have been used as inputs of the Monte Carlo simulations of 3.2 to fully describe the beam characteristics entering the sample.

3.2. Validation of the GEANT4 simulations against experimental measurements

In Figs. 2A and 2B, the comparison of the simulated PDDs with the experimental measurements is reported. The doses were normalised to 1 at 5 mm in depth along the z axis for an easier evaluation of the differences between the curves; 5 mm corresponds to the depth at which the ionisation chamber was placed, and hence the first available measurement. Solid lines show the simulated PDD, and therefore the percentage of dose found at different depths compared to the one delivered at 5 mm in depth; the red circles represent the PTW semiflex ionisation chamber measurements, while the blue triangles correspond to the film data. To better highlight the differences with the simulations, the bottom panels in Figs. 2A and 2B show the percentage difference ratios calculated as:

$$\%Difference = \frac{Dose(d)_{GEANT4} - Dose(d)_{\exp}}{Dose(d)_{\exp}} \cdot 100 \quad (3)$$

where $Dose(d)_{GEANT4}$ is the dose calculated at a specific depth with GEANT4, and $Dose(d)_{exp}$ is the dose at a specific depth measured with the PTW semiflex chamber or the EBT3 films. The experimental measurements are used as the reference term in both cases. In the bottom panels, the red circles correspond to the percentage difference between the ionisation chamber and the calculations, while the blue triangles give the differences between the film measurements and the simulations.

As expected, all the simulated dose profiles show a progressive attenuation with depth. For a given depth, the attenuation is less pronounced at higher energies (e.g., at 30 keV the dose at 100 mm is about 2–3% of the dose at 0.5 mm, while at 140 keV the dose is 26% at the same depth). The absolute doses obtained empirically show a comparable fall off, with maximum percentage difference obtained at 30 keV (about 5% at 10 cm depth) and 35 keV (about 6% at 6 cm depth) (Table 2). Overall, the dose measured with the chamber tends to be higher than the one measured with films. The agreement between simulations and experimental data is good overall, but the error diagrams reveal a tendency for GEANT4 to predict a more pronounced dose fall off than measured empirically at low energies at larger depths (30 mm or more at 30 keV, 40 mm or more at 35 keV), and a less pronounced fall off at higher energies. Before considering the contribution of high-order harmonics to the beam's energy compared to the monochromatic energy used in the simulations (results not shown), the disagreement between simulation and experiment was larger for lower energies, with differences of 32% and 19% for energies 30 and 35 keV, respectively. From 80 keV the tendency is opposite, and the calculated dose deposition is slightly lower than the measured one. All values reported in the Figures include already the high harmonic correction. In general, the agreement considerably improved with the inclusion of the harmonic contribution, staying within 9% for all the energies examined and for all depths; by considering depths < 60 mm, the agreement is within 5%.

3.3. The influence of high-Z materials on the PDD

For this part of the validation study the phantom shown in Fig. 1B was used. Our objective was to study the effect high-Z materials on dose deposition at different depths. The experimental measurements were carried out by filling the phantom with a water solution containing 10 mg/ml iodine or 4 mg/ml gadolinium. The same setup was simulated with GEANT4.

The resulting depth dose deposition profiles are reported in Fig. 3 for iodine and Fig. 4 for gadolinium. The solid lines represent the simulated results, with different colours denoting different energies. The points correspond to experimental measurements, with the same colour notation for different energies. For all five energy levels, experimental measurements were taken using the centre of the chamber at depths of 5, 39 and 73 mm, respectively. As before, both sets of measurements are normalised to the dose at 5 mm depth.

For all energies, the simulated data show both an underlying decreasing trend representing the reduction of the deposited dose as the beam travels through the phantom, and two spikes corresponding to when the beam travels through the containers filled with the high-Z solution. The experimental measurements confirm the predicted dose decrement giving a good match of the dose deposited in PMMA. In Fig. 3, at 30 keV, just below the iodine K-edge energy (33.17 keV), the increase in dose deposition as the beam enters the solution is about 75% compared to PMMA. Above the iodine K-edge, i.e. at 35 keV, the increase is about 150%. The higher dose enhancement is seen at 45 keV in the first solution container, where the increase is about 190%, and at 55 keV at a depth of 54 mm, which corresponds to the second container, where an increase of 80% can still be observed. At 75 keV an increase of 100% in the first container and 55% in the second can still be observed. In the case of gadolinium (Fig. 4), the dose enhancement observed is much lower because the concentration used is less than half of the iodine one, so a shorter vertical axis has been used to better evaluate the differences. Similarly to iodine, the maximum dose enhancement for gadolinium is seen at 55 keV, in the first container, and 55–75 keV in the second one, which is above the gadolinium K-edge energy (50.24 keV). If the gadolinium concentration is increased from 4 mg/l to 10 mg/ml (Fig. 5), the total dose enhancement increases (the vertical axis is now comparable with that of iodine in Fig. 3) and the monochromatic energy of 55 keV still gives the highest dose enhancement; however, this time the 75 keV beam is predominant in giving the highest dose enhancement in the second container. In general, for the same concentration of 10 mg/ml a higher dose enhancement in iodine than gadolinium can be observed, with differences of 40% at 21 mm, and 20% at 54 mm.

3.4. Dose enhancement factor

The DEF is computed as the ratio between the dose recorded when the two containers are filled with the high-Z solution and the dose recorded when they are filled with water. It is a useful metric to determine a scale of dose enhancement resulting from the use of the high-Z elements. Using our simulations, DEFs at energies of 30, 35, 45, 55 and 75 keV for both iodine and gadolinium were computed at a concentration of 10 mg/ml. The experimental data allow us to assess the corresponding DEFs outside the containers at depths of 5, 39 and 73 mm only for iodine, as the gadolinium concentration used experimentally was much lower.

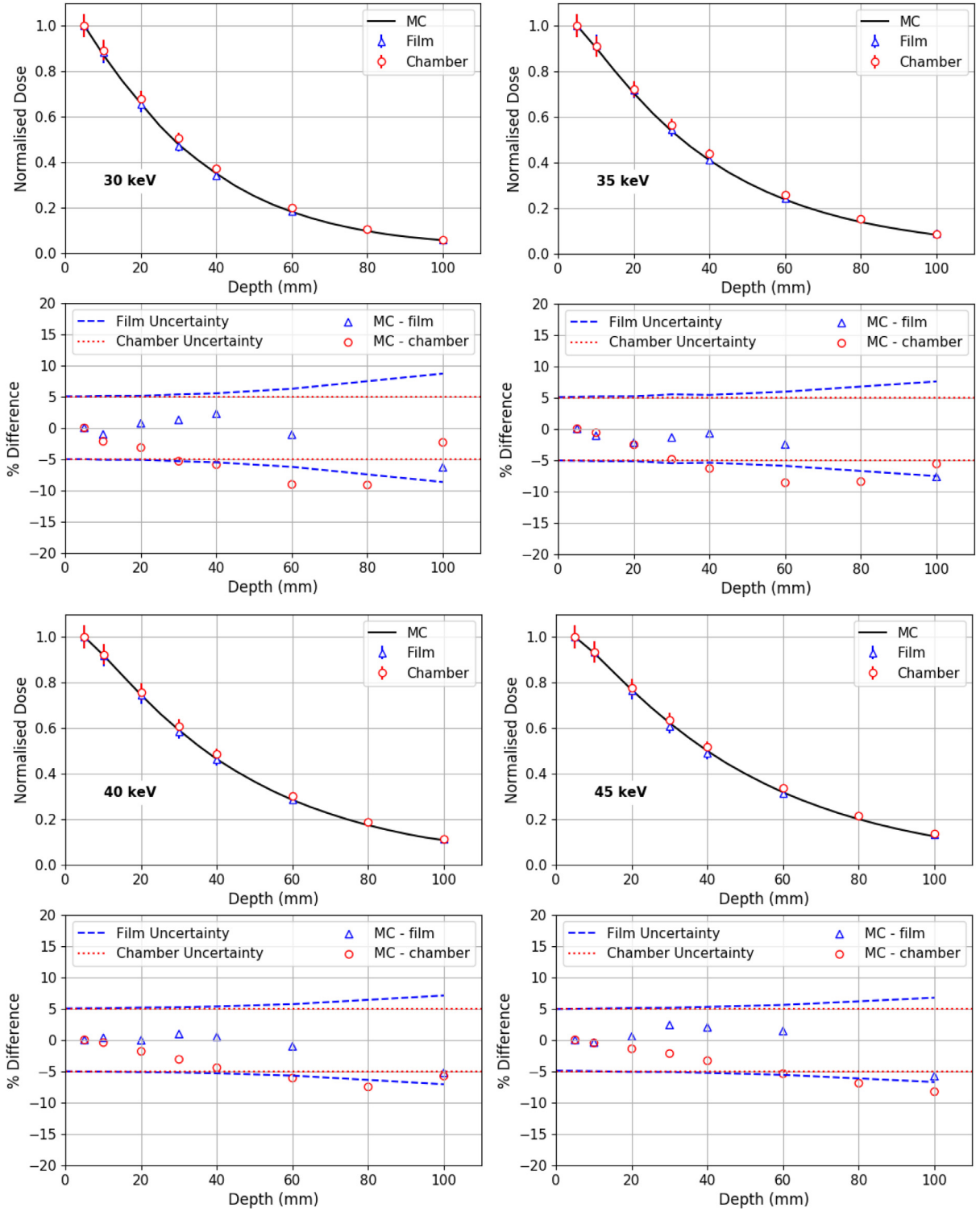

Fig. 2A. Top: The normalised experimental percentage depth dose acquired at different energies with the PTW semiflex ionisation chamber (red circles) and the EBT3 Gafchromic™ films (blue triangles) are compared with Monte Carlo simulations (solid lines). The experimental measurements are used as reference term in both cases. Bottom: percentage differences between data acquired with ionisation chamber and calculations (red circles), percentage differences between film measurements and calculations (blue triangles), and experimental uncertainties corresponding to the ionisation chamber (red dashed lines) and film measurements (blue dashed lines). (For interpretation of the references to colour in this figure legend, the reader is referred to the web version of this article.)

The decrease in DEF at larger depths, observed after the beam goes through the containers, represents the additional dose attenuation resulting from the larger number of interactions of the primary photons and especially secondary particles taking place inside each container when this is filled with a high-Z contrast medium. The results for iodine 10 mg/ml are reported in Fig. 6; the experimental measurements show that the GEANT4 code predicts that attenuation accurately. At energies just above the iodine K-edge, the fall-off after the beam enters the solution is very steep, while it becomes less prominent as the energy increases. With respect to dose enhancement, the effect is not

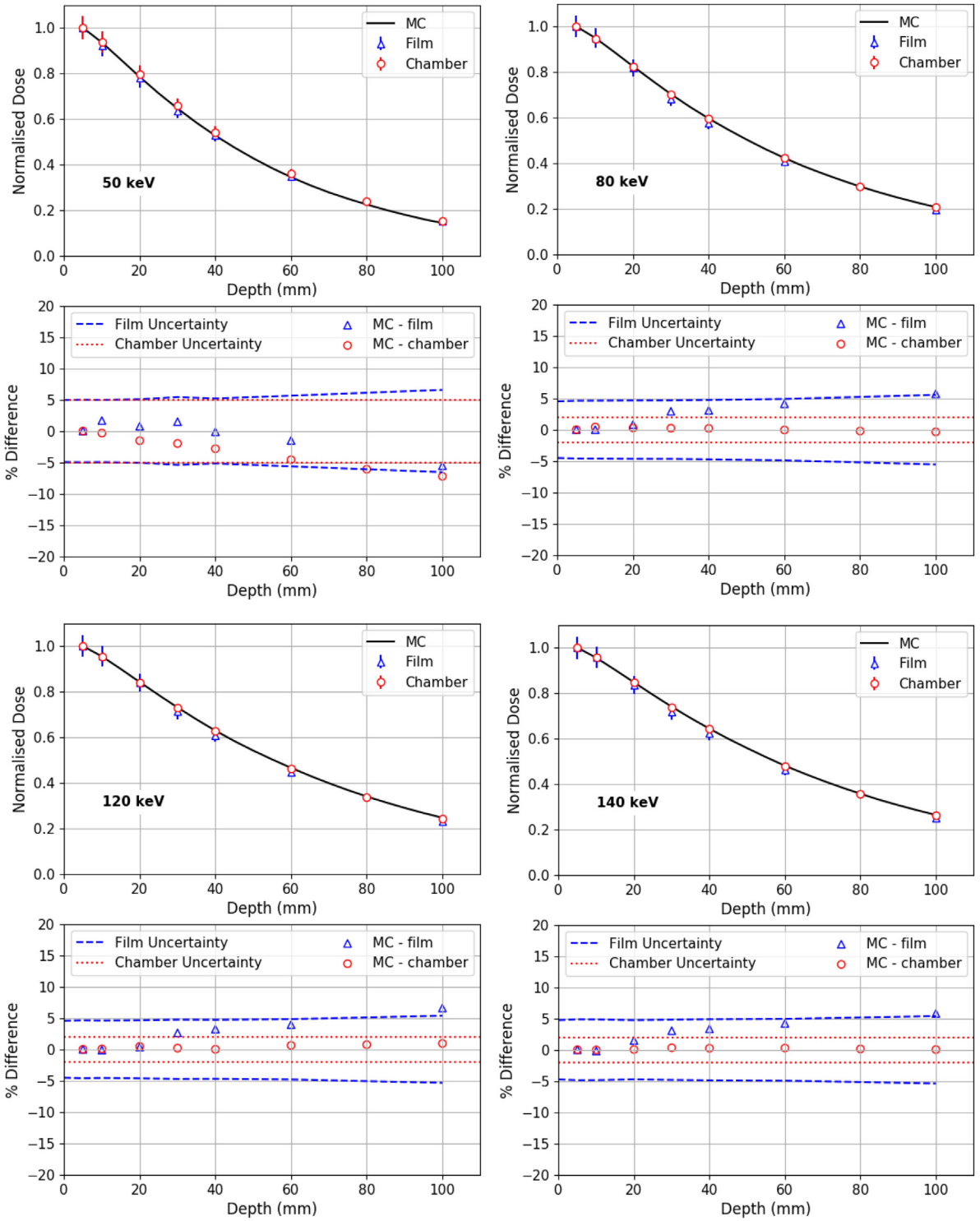

Fig. 2B. Top: The normalised experimental percentage depth dose acquired at different energies with the PTW semiflex ionisation chamber (red circles) and the EBT3 Gafchromic™ films (blue triangles) are compared with Monte Carlo simulations (solid lines). The experimental measurements are used as reference term in both cases. Bottom: percentage differences between data acquired with ionisation chamber and calculations (red circles), percentage differences between film measurements and calculations (blue triangles), and experimental uncertainties corresponding to the ionisation chamber (red dashed lines) and film measurements (blue dashed lines). (For interpretation of the references to colour in this figure legend, the reader is referred to the web version of this article.)

monotonically increasing in energy. In both containers, the largest effects were found at 55 keV, followed by 45, 75, 35 and 30 keV. The simulated DEFs for gadolinium at a concentration of 10 mg/ml are reported in Fig. 7. The fall-off when the beam goes through the solution is smoother than the one of iodine, with maximum DEFs reached for 55–75 keV in the first container and 75 keV in the second. The DEFs obtained inside the gadolinium compound are 20% lower than the ones achieved when using iodine.

DEFs were also calculated for different iodine concentrations, i.e. 5, 10 and 20 mg/ml, at 45 keV (Fig. 8A) and 55 keV (Fig. 8B), where the maximum depth dose deposition has been previously found. The DEFs profiles at different concentrations show a similar trend. A spike can be

Table 2
Percentage differences in experimental dose measurements acquired at different energies with EBT3 and semiflex chamber. The film measures are considered as reference term.

Energy/depth (mm)	30 keV	35 keV	40 keV	45 keV	50 keV	80 keV	120 keV	140 keV
10	0.6	−0.3	1.5	−0.1	2.1	−0.2	0.1	−0.2
20	1.6	0.02	2.0	1.0	2.1	0.3	0.2	0.9
30	1.7	3.4	4.2	3.9	4.3	2.2	2.5	2.2
40	0.5	5.6	5.4	4.3	3.8	2.8	2.9	3.1
60	−0.8	6.1	5.3	6.1	5.2	3.8	1.8	3.2
100	−4.7	−1.3	1.4	3.8	4.3	4.0	0.9	1.3

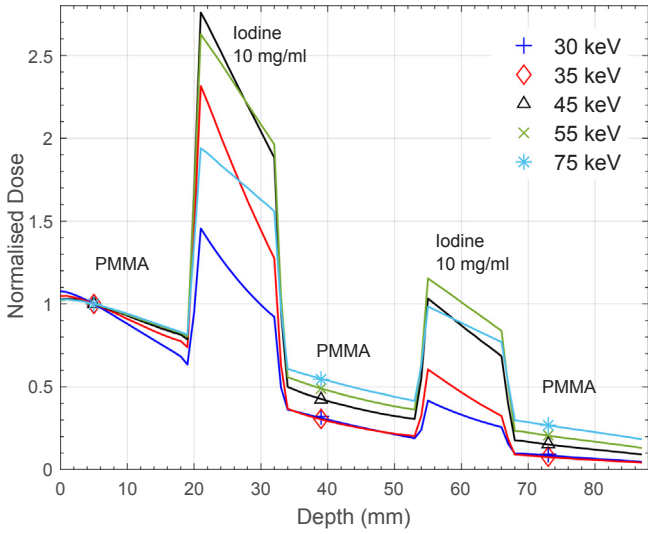

Fig. 3. Dose deposition at different energies when filling the phantom with an iodine solution at 10 mg/ml. The solid lines represent the simulated results. The points correspond to experimental measurements. Different colours denote different energies. All sets of measurements are normalised to the dose at 5 mm in depth. (For interpretation of the references to colour in this figure legend, the reader is referred to the web version of this article.)

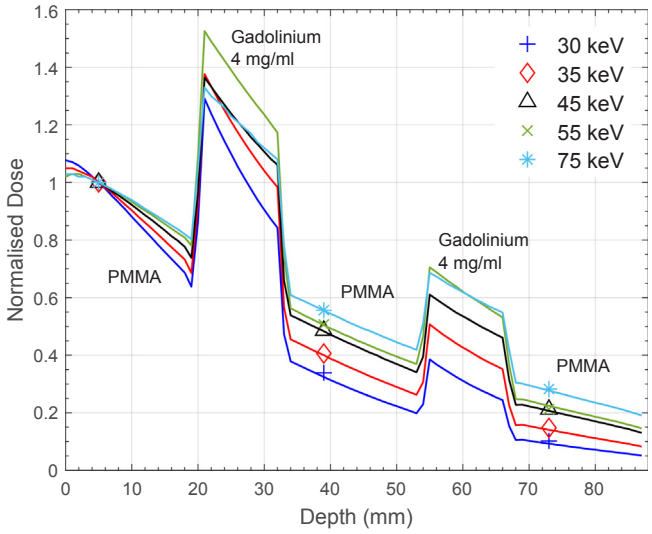

Fig. 4. Dose deposition at different energies when filling the phantom with a gadolinium solution at 4 mg/ml. The solid lines represent the simulated results. The points correspond to experimental measurements. Different colours denote different energies. All sets of measurements are normalised to the dose at 5 mm in depth. (For interpretation of the references to colour in this figure legend, the reader is referred to the web version of this article.)

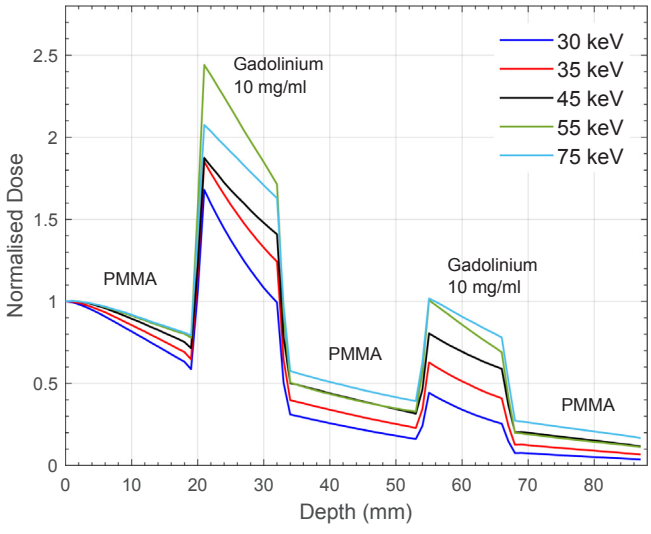

Fig. 5. Dose deposition at different energies when filling the phantom with a gadolinium solution at 10 mg/ml.

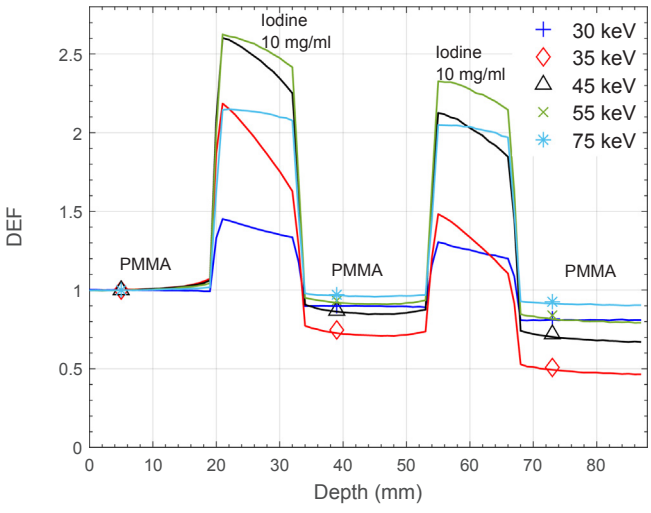

Fig. 6. Dose enhancement factors calculated with GEANT4 (solid lines) and benchmarked experimentally in PMMA (points) using an iodine solution 10 mg/ml as dose enhancer. Different colours denote different energies.

noticed as the beam enters the solution (at about 20 and 54 mm depth, respectively), followed by a gradient of dose fall-off as the radiation travels inside the solution. Higher concentrations give a maximum DEF and show a steeper fall-off gradient due to the beam attenuation. The 45 keV beam produces steeper spikes and lower DEFs compared to the 55 keV beam, with differences up to 40% in the second container at a depth of 54 mm.

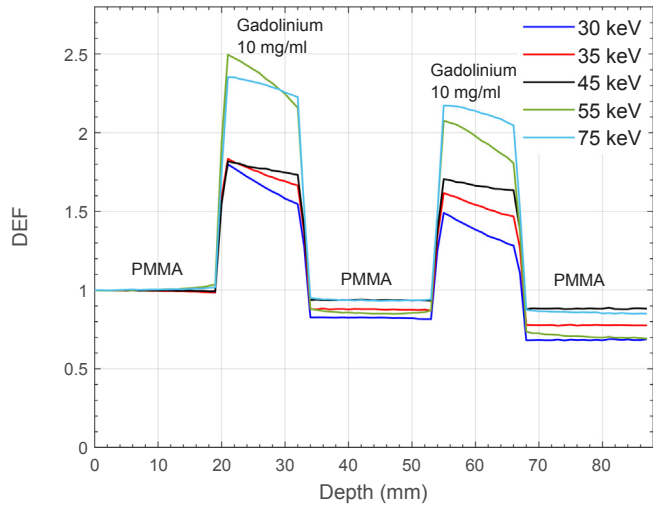

Fig. 7. Dose enhancement factors calculated with GEANT4 in a gadolinium solution at 10 mg/ml.

4. Discussion

The use of high-Z compounds has gained increasing interest in radiotherapy due to the observed dose enhancement after photon irradiation. This effect is particularly evident when using beams in the kiloelectronvolt energy range as photons have energy closer to the K-shell binding energy of the high-Z materials. At such energies, photons interact mainly via photoelectric absorption and Compton scattering, both leading to the production of secondary electrons, which contribute, therefore, to the local dose deposition in the vicinity of the high-Z compound. In water, photoelectric absorption is prevalent at very low energies, while above about 30 keV Compton scattering becomes dominant [24]. At the energy range considered, secondary electrons travel for 0.01–1 mm in water, so they will deposit their energy locally. As a consequence, the shape of the depth dose curve depends largely on the attenuation of primary photons and the dose deposition of scattered photons.

In this work, we explored the suitability of GEANT4 to be used as a Monte Carlo toolkit for dose enhancement studies when using synchrotron generated uniform monochromatic beams. We compared the theoretical results with experimental measurements acquired via a PTW semiflex ionisation chamber and EBT3 Gafchromic™ film. The experimental absolute doses (considered before the normalisation) stayed within the statistical uncertainty at all energies. When using the RW3 commercial slab phantom, the simulated depth dose curves compared well with the experimental measurements apart from lower energies. We found that this was due to the presence of high-order harmonics, making up a non-trivial component to the beam energy compared to the monochromatic energy used in the simulations. We quantified the harmonic contribution and found the highest contamination at 30 keV, i.e. up to 2.5% of the fundamental energy at the entrance of the sample. The harmonic contribution on the incoming beam decreased with energy, being up to 0.98% at 40 keV. Considering how the percentage differences were calculated, it is worth highlighting that the differences look larger at lower energies because we were dividing for a smaller number, being the dose at 10 mm lower for 30 keV than for higher energies. The same behaviour was in fact observed considering the measured absolute doses (film compared to ionisation chamber), where the highest discrepancies of up to 6% were also found at the lowest energies of 30 keV and 35 keV. The ionisation chamber differences were more pronounced for lower energies (30–45 keV), while the agreement for higher energies (80–140 keV) was within 2%. The agreement with the film was inside the uncertainty region for most of the energies.

After filling the phantom with the high-Z compound, as expected, the depth dose curves did not show a simple decreasing trend following the Beer-Lambert law. We used concentrations mimicking the local contrast agent concentrations found in the literature [30,31,32]. A dose enhancement was found inside the metal-based mixtures for all studied energies. The dose was not measured experimentally inside the liquid due to the lack of a commercial dosimeter of appropriate thickness to produce meaningful results. In fact, the same high-Z effect that justifies the high specificity of the dose distribution (short distance travelled by the photoelectrons, characteristic X-rays and Auger electrons) also makes the dose enhancement generated by these agents difficult to measure. The laminated radiochromic films have in fact a polyester layer that, although very thin (i.e. 125 μm for EBT3 films) would stop the secondary electron generated, giving a lower detected dose deposition. On the other hand, the use of unlaminated films, such as the HD-V2, is unmanageable as the active layer would dissolve into the solution.

Calculating the depth dose curves was the first essential step in order to determine the DEF, which is defined as the ratio between the dose to water with enhancers and the dose to water alone. For iodine 10 mg/ml, the simulations showed the highest dose enhancement at 45 keV when the beam enters the solution in the first container, and at 55 keV in the second one. The highest DEF was found at 55 keV, followed by 45 keV. These results look interesting considering that the iodine K-edge corresponds to an energy of 33.17 keV. An explanation of this fact can be found by looking at the mass energy absorption coefficient in water and iodine, which involves the absorption not only of the primary photons, but also of the secondary particles produced by the primary photons when travelling through the medium. Roeske *et al.* [33] showed that the DEF is directly proportional to the ratio of the mass energy absorption coefficient in the dose enhancer with a given concentration and the same coefficient in water; this occurs when a

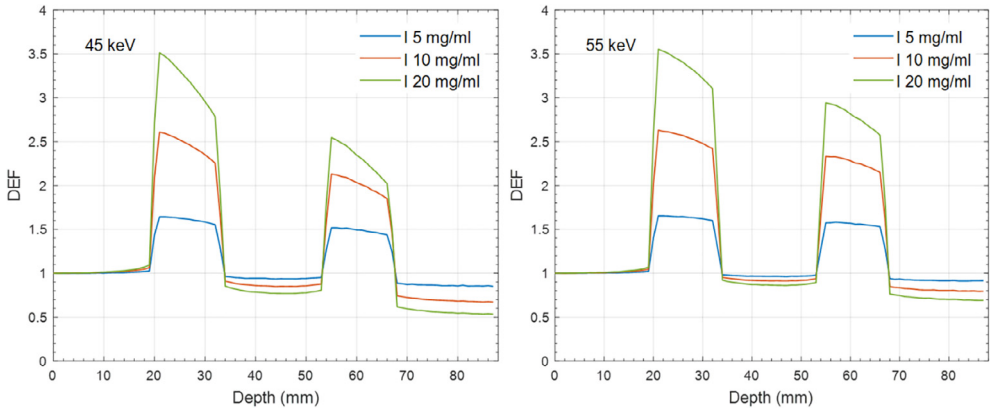

Fig. 8. Dose enhancement factors calculated with GEANT4 at 45 keV (A) and 55 keV (B) using different iodine concentrations.

monochromatic photon beam is used, the density in the irradiated medium is uniform, and under conditions of charged particle equilibrium. At the energies considered in this study, this ratio has a maximum at about 50 keV [24], which is in line with our results. By considering different iodine concentrations, we found higher DEFs at higher concentrations, due to an increased number of secondary interactions in iodine compared to water, while the calculated dose deposition in PMMA has the opposite trend (it decreases as the concentration increases). As far as the gadolinium is concerned, the highest dose enhancement was seen at 55 keV in the first container and 75 keV in the second one. The highest DEFs were also found at 55 keV and 75 keV. This is in line with what found for iodine, if we consider that the gadolinium K-edge energy is higher and equal to 50.24 keV. In general, for equal concentrations, we found higher DEFs in iodine than gadolinium.

5. Conclusion

This study investigated the use of GEANT4 as a Monte Carlo simulation tool to predict the dose distributions at low energies when using a uniform monochromatic synchrotron-generated X-ray beam in different experimental configurations. The final goal was to assess via simulations the potential dose enhancement given by the introduction of high-Z compounds in a phantom irradiated with targeted keV radiation, with some measurements to enable a comparison with the model. We considered the PDD obtained with the irradiation of a commercial PTW RW3 phantom, and benchmarked the results against experimental measurements acquired at the ESRF with two different dosimeters such as a PTW semiflex chamber and EBT3 Gafchromic™ films. The contribution of high-order harmonics to the incoming beam was quantitatively assessed for the monochromatic energies in the range 30–40 keV, and an agreement within 9% was found among simulations and empirical data for all the monochromatic energies considered. At low energies, the highest discrepancy (within 6%) was found between the absolute dose measured with the ionisation chamber and the one measured with films at higher depths (6–10 cm), highlighting the difficulty in dealing with such small doses.

We considered the effect of the introduction of high-Z regions in a PMMA phantom, by filling two containers with iodinated and gadolinium-based compounds, for different concentrations and incident X-ray energies. The calculations clearly emphasised a dose enhancement in the contrast medium areas, and the experimental measurements carried out in PMMA just before or after those regions overlapped the depth dose deposition simulated with GEANT4. The dose enhancement factors were used to evaluate the increase of the dose in the phantom. Results of this study indicate that DEFs are both photon energy- and concentration- dependent, and the highest DEFs are found for energies not immediately above the K-edge, but slightly higher. According to the results, a rapid increase in the DEF values is obtained with increased concentrations; however, in accordance with the literature, using conventional (i.e. not nano-particle based) high-Z contrast agents, it is difficult to reach concentrations in tissues larger than 10 mg/ml [32], due to the tolerance limit set by healthy organs. The results of this work support the use of GEANT4 as a tool for the calculation of the PDD at low energies in the presence of contrast agents.

Acknowledgements

The Authors are thankful to ESRF for providing synchrotron radiation through the proposal MD1144 and to the biomedical beamline team, especially Mrs. Alexandra Demory, Dr. Herwig Requardt and Mrs. Mariele Romano for their help during the experiment. The GEANT4 developers attending the Third GEANT4 International User Conference are thanked for the fruitful discussions. The STFC and the Global Challenge Network + in Advanced Radiotherapy are kindly acknowledged for funding. This study was supported by the Daphne Jackson Trust and the EPSRC, which are kindly acknowledged. This study was also supported by the Swedish Research Council (grant nr. X2015-99x-22731-01-4).

References

[1] Karnas SJ, Moiseenko VV, Yu E, Truong P, Battista JJ. Monte Carlo simulations and measurement of DNA damage from X-ray-triggered auger cascades in iododeoxyuridine (IUdR). Radiat Environ Biophys. 2001;40(3):199–206.
[2] Terrissol M, Edel S, Pomplun E. Computer evaluation of direct and indirect damage induced by free and DNA-bound iodine-125 in the chromatin fibre. Int J Radiat Biol. 2004;80(11-12):905–8.
[3] Taupin F, Flaender M, Delorme R, Brochard T, Mayol JF, Arnaud J, et al. Gadolinium nanoparticles and contrast agent as radiation sensitizers. Phys Med Biol 2015;60(11):4449–64.
[4] Chithrani DB, Jelveh S, Jalali F, van Prooijen M, Allen C, Bristow RG, et al. Gold nanoparticles as radiation sensitizers in cancer therapy. Radiat Res. 2010;173(6):719–28.
[5] Lechtman E, Mashouf S, Chattopadhyay N, Keller BM, Lai P, Cai Z, et al. A Monte Carlo-based model of gold nanoparticle radiosensitization accounting for increased radiobiological effectiveness. Phys Med Biol 2013;58(10):3075–87.
[6] Zhang DG, Feygelman V, Moros EG, Latifi K, Zhang GG. Monte Carlo study of radiation dose enhancement by gadolinium in megavoltage and high dose rate radiotherapy. PLoS ONE 2014;9(10):e109389.
[7] Robar JL. Generation and modelling of megavoltage photon beams for contrast-enhanced radiation therapy. Phys Med Biol 2006;51(21):5487–504.
[8] Ceresa C, Nicolini G, Requardt H, Le Duc G, Cavaletti G, Bravin A. The effect of Photon Activation Therapy on cisplatin pre-treated human tumour cell lines: comparison with conventional X-ray irradiation. J Biol Regul Homeost Agents 2013;27(2):477–85.
[9] Ceresa C, Nicolini G, Semperboni S, Requardt H, Le Duc G, Santini C, et al. Synchrotron-based photon activation therapy effect on cisplatin pre-treated Human Glioma stem cells. Anticancer Res. 2014 Oct;34(10):5351–5.
[10] Ceresa C, Bravin A, Cavaletti G, Pellei M, Santini C. The combined therapeutical effect of metal-based drugs and radiation therapy: the present status of research. Curr Med Chem 2014;21:2237–65.
[11] Corde S, Balosso J, Elleaume H, Renier M, Joubert A, Biston MC, et al. Synchrotron photoactivation of cis-platin (PAT-Plat) elicits an extra-number of DNA breaks that stimulate RAD51-mediated repair pathways. Cancer Res 2003;63:3221–7.
[12] Corde S, Joubert A, Adam JF, Charvet AM, Le Bas JF, Esteve F, et al. Synchrotron radiation-based experimental determination of the optimal energy for cell radiotoxicity enhancement following photoelectric effect on stable iodinated compounds. Br J Cancer 2004;91:544–51.
[13] Seiwert TY, Salama JK, Vokes EE. The concurrent chemoradiation paradigm–general principles. Nat Clin Pract Oncol. 2007;4(2):86–100.
[14] Solberg TD, Iwamoto KS, Norman A. Calculation of radiation dose enhancement factors for dose enhancement therapy of brain tumours. Phys Med Biol 1992;37:439.
[15] Verhaegen F, Reniers B, Deblois F, Devic S, Seuntjens J, Hristov D. Dosimetric and microdosimetric study of contrast-enhanced radiotherapy with kilovolt x-rays. Phys Med Biol 2005;50:3555.
[16] Morris KN. Radiochromic film dosimetry of contrast-enhanced radiotherapy (CERT). Phys Med Biol 2006;51:5915.
[17] Prezado Y, Fois G, Le Duc G, Bravin A. Gadolinium dose enhancement studies in microbeam radiation therapy. Med Phys 2009;36:3568–74.
[18] Engels E, Corde S, McKinnon S, Incerti S, Konstantinov K, Rosenfeld A, et al. Optimizing dose enhancement with Ta2O5 nanoparticles for synchrotron microbeam activated radiation therapy. Phys Med. 2016;32(12):1852–61. https://doi.org/10.1016/j.ejmp.2016.10.024. Epub 2016 Nov 17.
[19] McKinnon S, Engels E, Tehei M, Konstantinov K, Corde S, Oktaria S, Incerti S, Lerch M, Rosenfeld A, Guatelli S. Study of the effect of ceramic Ta2O5 nanoparticle distribution on cellular dose enhancement in a kilovoltage photon field. Phys Med 2016;32(10):1216–24. https://doi.org/10.1016/j.ejmp.2016.09.006. Epub 2016 Sep 22.
[20] Allison J, et al. Recent developments in GEANT4. Nucl Instrum Meth A 2016;835:186–225.
[21] Bravin A, Fiedler S, Coan P, Labiche J-C, Ponchut C, Peterzol A, et al. Thomlinson Comparison between a position sensitive germanium detector and a taper optics CCD "FRELON" camera for Diffraction Enhanced Imaging. Nucl Inst Meth 2003;A510:35–40.
[22] Suortti P, Fiedler S, Bravin A, Brochard T, Mattenet M, Renier M, Spanne P, Thomlinson W, Charvet AM, Elleaume H, Schulze-Briese C, Thompson AC. Fixed-exit monochromator for computed tomography with synchrotron radiation at energies 18-90 keV. J Synchrotr Radiat 2000;7(Part 5):340–7.
[23] Sanchez del Rio M, Dejus JR. XOP v2.4: Recent developments of the X-ray optics software toolkit. Proc SPIE 2011;8141.
[24] NIST online database. < https://www.nist.gov/pml/x-ray-mass-attenuation-coefficients > .
[25] Seuntjens J, Olivares M, Evans M, Podgorsak E. Absorbed dose to water reference dosimetry using solid phantoms in the context of absorbed-dose protocols. Med Phys 2005;32:2945–53.
[26] Cameron M, Cornelius I, Cutajar D, Davis J, Rosenfeld A, Lerch M, et al. Comparison of phantom materials for use in quality assurance of microbeam radiation therapy. J Synchrotron Rad 2017;24:866–76.

[27] < http://www.gafchromic.com/documents/EBT3_Specifications.pdf. > .
[28] Prezado Y, Vautrin M, Martínez-Rovira I, Bravin A, Estève F, Elleaume H, et al. Dosimetry protocol for the forthcoming clinical trials in synchrotron stereotactic radiation therapy (SSRT). Med Phys 2011;38(3):1709–17.
[29] Devic S, Tomic N, Lewis D. Reference radiochromic film dosimetry: review of technical aspects. Phys Med 2016;32(4):541–56.
[30] Le Duc G, Corde S, Elleaume H, Estève F, Charvet AM, Brochard T, et al. Feasibility of synchrotron radiation computed tomography on rats bearing glioma after iodine or gadolinium injection. Eur Radiol 2000;10(9):1487–92.
[31] Adam J-F, Nemoz C, Bravin A, Fiedler S, Bayat S, Monfraix S, et al. High-resolution blood−brain barrier permeability and blood volume imaging using quantitative synchrotron radiation computed tomography: study on an F98 rat brain glioma. J Cer Blood Flow Met 2005;25:145–53.
[32] Obeid L, Deman P, Tessier A, Balosso J, Estève F, Adam J-F. Absolute perfusion measurements and associated iodinated contrast agent time course in brain metastasis: a study for contrast-enhanced radiotherapy. J Cer Blood Flow Met 2014;34:638–45.
[33] Roeske JC, Nunez L, Hoggarth M, Labay E, Weichselbaum RR. Characterization of the theorectical radiation dose enhancement from nanoparticles. Technol Cancer Res Treat 2007;6(5):395–401.